Size-Topology Relations in Packings of Grains, Emulsions, Foams, and Biological Cells

K. A. Newhall,[1] L. L. Pontani,[2] I. Jorjadze,[2] S. Hilgenfeldt,[3] and J. Brujic[2]

[1]*New York University, Courant Institute of Mathematical Sciences, 251 Mercer Street, New York, New York 10012, USA*

[2]*New York University, Department of Physics and Center for Soft Matter Research, 4 Washington Place, New York, New York 10003, USA*

[3]*Mechanical Science and Engineering, University of Illinois at Urbana Champaign, 1206 W Green Street, Urbana, Illinois 61801, USA*

(Received 17 April 2012; published 26 June 2012)

Particulate packings in 3D are used to study the effects of compression and polydispersity on the geometry of the tiling in these systems. We find that the dependence of the neighbor number on cell size is quasilinear in the monodisperse case and becomes nonlinear above a threshold polydispersity, independent of the method of creation of the tiling. These size-topology relations can be described by a simple analytical theory, which quantifies the effects of positional disorder in the monodisperse case and those of size disorder in the polydisperse case and is applicable in two and three dimensions. The theory thus gives a unifying framework for a wide range of amorphous systems, ranging from biological tissues, foams, and bidisperse disks to compressed emulsions and granular matter.

DOI: 10.1103/PhysRevLett.108.268001 PACS numbers: 45.70.−n, 45.70.Vn, 81.05.Rm, 82.70.Rr

Systems that tile space range from tessellations of particulate packings [1–4] to soap foams [5–10], biological tissues [11–13], and even mathematically generated tilings [14]. In each of these systems, the size distribution, topology, and dimensionality of the constituent cells determine the relation between the number of neighboring cells and the cell size [15,16]. For example, this relationship is linear in the case of the empirical Lewis law [11] observed in epithelial tissues from organisms as diverse as the Drosophila wing, Xenopus tadpole tail, Hydra vulgaris, or the cucumber epidermis, but it follows a power law in the case of foam tilings [9,10,17]. While many theoretical approaches have been devised to predict a specific size-topology trend [17–22], none have been able to explain the origin of the discrepancy between systems or quantify the limits of validity of different size-topology relations. Another open question is how these relations are affected by the dimensionality of the system, given that structural information inside 3D tilings is difficult to access. To this end, we confocally image transparent, fluorescent particulate packings ranging from monodisperse poly-methylmethacrylate (PMMA) particles to compressed emulsion droplets with varying polydispersity. The individual cells in the mosaic are constructed either by tessellating space around spheres using the navigation map [23,24] or by physical compression of the particles themselves. We find that the monodisperse particles follow a different size-topology relation to the polydisperse emulsions, independent of the method of creation of the tiling.

Building on the work in [22], we derive analytical results from simplified versions of the granocentric model [1,25] for the size-topology relations to explain the diverse data in 2D and in 3D. This idealized model is based on creating individual cells in the tiling by surrounding a central particle with a first shell of neighbors. Variations in the particle sizes introduce disorder arising from polydispersity, while fluctuations in the surface-to-surface distance between the neighbors mimic positional disorder in the packing. This model allows us to decouple the two effects and distinguish between systems where the particles are all of the same or similar size but the distance between them can vary (i.e. positional disorder) and those where the size-distribution of the particles (i.e., polydispersity) dominates the disorder in the tiling. We find that the analytical predictions of the model capture experimental trends in systems as diverse as biological tissues, bubbles, droplets, and grains and, thus, classify them according to the dominant source of disorder in their packing.

Figure 1 depicts examples of amorphous tilings, ranging from epithelial cells and bidisperse disks in 2D to confocal slices of compressed and relaxed emulsions in 3D. The emulsion packings are visualized in 3D by refractive index matching the droplets with the continuous phase and dying the particles using fluorescent Nile Red dye. The image analysis, based on a Fourier transform algorithm, identifies the particle positions and radii [26]. Note that the cells are either defined by the space filling of deformable particles as in Figs. 1(a) and 1(c) or by the navigation map tessellation of space [23,24] around circular or spherical particles as shown in Figs. 1(b) and 1(d). The navigation map tessellation attributes each point in space to the particle whose surface is closest to it. In the monodisperse case, this method reduces to the Voronoi tessellation. In the polydisperse case, this method results in individual cell volumes separated by hyperbolic surfaces. In either case, the number of neighbors n is defined as the number of interfaces that a cell shares with other cells. In 2D, the cellular tissues and jammed disks follow the linear law proposed by Lewis,

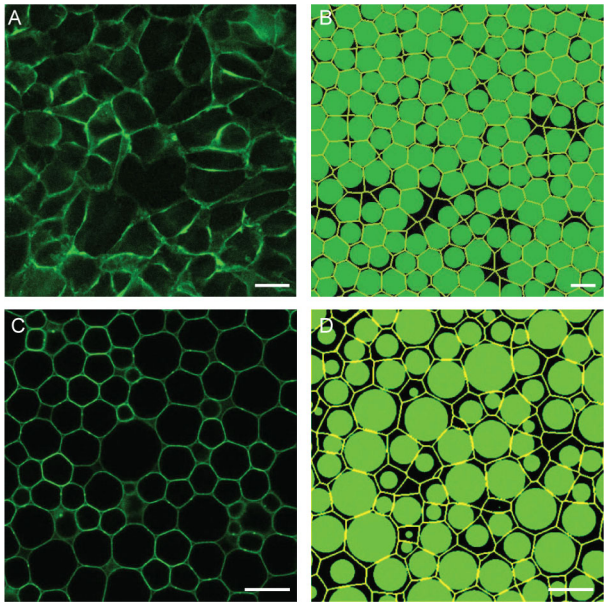

FIG. 1 (color online). Tilings of space-filling systems and tessellations of particulate packings. In 2D, epithelial tissue of MDCK cells stained with GFP fused E-cadherin (scale bar = 10 μm) shown in (a) is compared with a random packing of bidisperse disks segmented by the navigation map shown in (b) (scale bar = 2.2 cm). The 2D confocal images in (c) and (d) represent slices of the 3D tessellations of spheres achieved by the compression of polydisperse droplets ($p = 22\%$) and the tessellation of the undeformed droplets, respectively (scale bar = 10 μm).

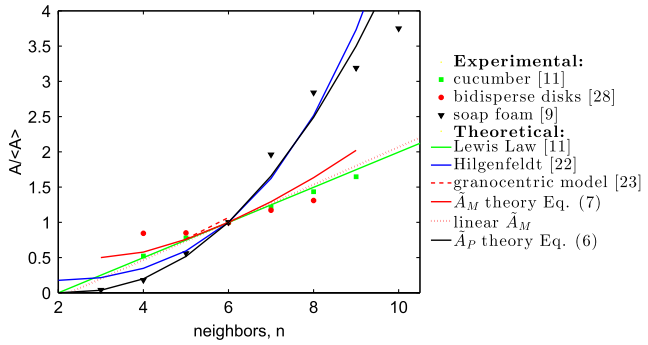

FIG. 2 (color online). For 2D systems, the relationship between the average area of cells with n neighboring cells and n is shown. Lewis' cucumber data and law $A/\langle A\rangle = 1 + 0.246(n - 6)$ [11]. Bidisperse discs with size ratio 1.22 chosen to avoid crystallization [30].

while the foam data follow a nonlinear increase with the cell area, as shown in Fig. 2. A similar distinction is observed for the dependence of the average cell volume V on neighbor number in packings of monodisperse PMMA particles and polydisperse emulsions in 3D, as shown in Fig. 3(a). Interestingly, varying the level of polydispersity p (where p is the coefficient of variation of the droplet radii) from 11% to 42% in 3D packings of emulsion droplets does not change the nonlinear shape of the relationship between neighbor number and cell volume. In addition, compressing the deformable droplets by centrifugation into a biliquid foam structure does not significantly change the size-topology relation. This observation suggests that it is appropriate to use a theory for packings of spherical particles and apply the results to space-filling systems.

We, therefore, apply the granocentric model for packing particles [25] to our data. This model maps the packing process onto a first passage problem of a one-dimensional random walk in solid angle space by adding the sold angle contributions of the first shell of neighbors of a given particle. A second random process chooses some of these neighbors to be in contact with the central particle to ensure mechanical stability, while the others are placed a given surface-to-surface distance away. This model is capable of describing local fluctuations in the neighbor number and volume of cells within jammed packings of hard spheres with any size distribution. As shown in Figs. 2 and 3 by the dashed lines, the model is in excellent agreement with the distinctive differences between the size-topology relations in monodisperse and polydisperse packings, both in 2D and in 3D. The model, however, does not give systematic insight into the origins of the discrepancy, nor into the remarkable universal character of the size-topology relation above a certain critical polydispersity (Figs. 2 and 3). Therefore, we introduce a mean-field approximation of the granocentric model, allowing us to decouple polydispersity and positional effects. We assume all neighbors of a given central particle of radius r_c are of the same size, μ_r, corresponding to the average of the size distribution in the packing. In the polydisperse case, we vary r_c to obtain the effect of the particle size on the number of neighbors. Positional disorder is neglected in this case because all the particles are assumed to be in contact with the central particle. In the case of monodisperse packing (where $r_c = \mu_r$), we place all the neighbors in a given cell at a distance $\delta\mu_r$ away from the surface of the center particle. We then vary δ to analyze the effect of positional disorder. In this way, we isolate the effect of two sources of randomness found in packings and deduce their influence on the cell area or volume independently.

The relation between the number of neighbors n and either r_c/μ_r or δ follows from dividing the total available solid angle, $\Omega_{\max}$, around the central particle, among these n neighbors. A simple calculation shows that in 3D

$$n = \frac{\Omega_{\max}}{2\pi}\left(1 - \frac{\sqrt{(1+\xi)^2 - 1}}{1+\xi}\right)^{-1} \qquad (1)$$

where $\xi = r_c/\mu_r$ for size disorder and $\xi = 1 + \delta$ for positional disorder. In this expression, $\Omega_{\max}$ is adjusted so that the average number of neighbors $\langle n\rangle$ takes a given value, which is close to 14 for many random particulate packings. This value has been shown to be insensitive to polydispersity [1,27] and the interaction potential between

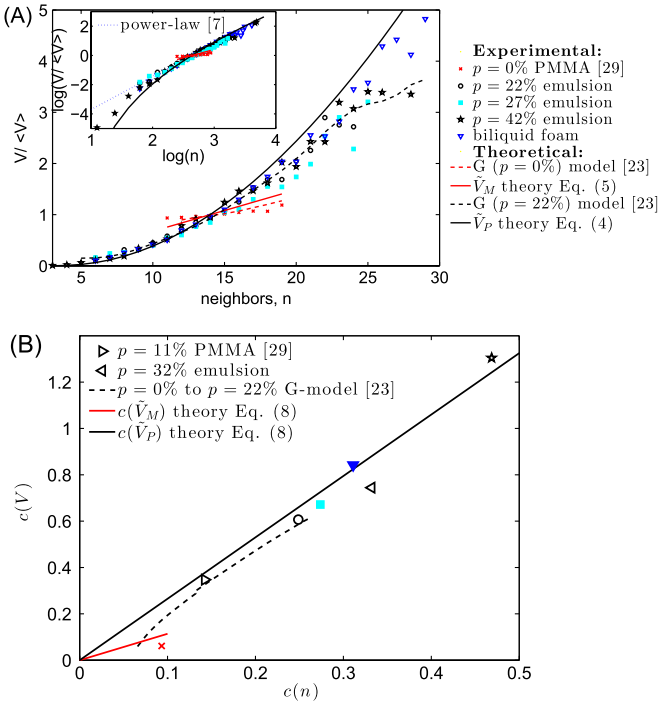

FIG. 3 (color online). For 3D systems, (a) depicts the relationship between the average volume and n. This is plotted on a log-log scale in the inset, where the blue dotted line is the power-law fit (slope of 2.262) to the random 3D foam from Kraynik *et. al* [7]. (b) The relationship between widths of neighbor-number and cell-volume distributions. Each point represents one experiment; the legend indicates additional experiments not shown in (a). The dashed line is obtained from the granocentric model [25] by varying the particle size distribution from monodisperse ($p = 0\%$) to 22% polydispersity.

the particles [2]. In principle, $\langle n\rangle$ must be calculated by averaging (1) over the particle size distribution of r_c or over the distribution of δ. We can bypass this calculation by setting $\xi = 1$ in (1), corresponding to the case of equal-sized spheres that are touching each other, to obtain the leading order term of $\langle n\rangle$. This gives $\Omega_{\max} \approx (2 - \sqrt{3})\pi\langle n\rangle \approx 3.75\pi$ for $\langle n\rangle = 14$.

Following the prescription of the granocentric model, we approximate the cell volume generated by the navigation map tessellation by having each neighbor contribute the volume of a conic section with a hyperbolic cap defined by the points equidistant from both particle surfaces [28]. Summing over these neighbor contributions, as well as the central particle volume, then gives the total volume of the cell. With size disorder where $\xi = r_c/\mu_r$, the resulting cell volume, V_P, for polydisperse packings is

$$V_P = \frac{4\pi r_c^3[2n - (1 + \xi)]}{6[n - (1 + \xi)]^2}, \tag{2}$$

and with positional disorder where $\xi = 1 + \delta$, the resulting cell volume, V_M, for monodisperse packings is

$$V_M = \frac{4\pi r_c^3(1 + \xi)^3 n(n - 1)}{24(n - 2)^2}. \tag{3}$$

Using (1) to express ξ in terms of n in (2) gives an analytical prediction for the volume of cells with n neighbors in a polydisperse packing,

$$\tilde{V}_P = \left(\frac{2n}{a(n)} - 1\right)^3 \left(\frac{a^2(n) - a(n)}{\langle n\rangle^2 - \langle n\rangle}\right)\left(\frac{\langle n\rangle - 2}{a(n) - 2}\right)^2, \tag{4}$$

where $\tilde{V}_P \equiv V_P/\langle V\rangle$ is the cell volume normalized to the average volume, and $a(n) = 2\sqrt{2k\langle n\rangle n - k^2\langle n\rangle^2}$ with $k = 1 - \sqrt{3}/2$. The relation in (4) with $\langle n\rangle = 14$, which varies little for any realistic $\langle n\rangle$, agrees well with the compressed and relaxed emulsion data with a wide range of polydispersities, as shown in Fig. 3(a). This agreement implies that size-induced disorder captured by the model dominates over the positional disorder also present in these experimental packings. The universality among a range of polydisperisities arises because polydispersity only affects the range of n through the parameter ξ, but not the functional relationship between V_P and n, which is fixed after the elimination of ξ. While previous theoretical work had conjectured $\tilde{V}_P \propto n^\beta$ with $\beta = 3$ [29] and empirical data from foam simulations were well described by $\beta \approx 2.25$ [7], our theory indicates that this relation is more complex than a power law. In fact, a useful simplified relation can be obtained through expansion of (4) in $\sqrt{n}$, which for $\langle n\rangle = 14$ gives to excellent approximation for all n, $\tilde{V}_P \approx 0.12n^{3/2} - 0.55n + 0.94n^{1/2} - 0.55$, with an intuitive asymptotic scaling of $\tilde{V}_P \propto n^{3/2}$ as $n \to \infty$.

Similarly, we can eliminate ξ between (1) and (3) to obtain a relationship between cell volume and neighbor number in the positional disorder case. Since in monodisperse packings the range of n is very restricted (typically $11 \le n \le 18$), a linear expansion around $n = \langle n\rangle$ is sufficiently accurate and gives

$$\tilde{V}_M = 1 + g_M(n - \langle n\rangle), \tag{5}$$

where the slope g_M varies only weakly with $\langle n\rangle$ and, for $\langle n\rangle = 14$, is ≈ 0.081. Thus, for monodisperse packings, $\tilde{V}_M$ is much less sensitive to n, as shown by the red solid line in Fig. 3(a). The analytical approach using only one value of δ per cell does not model the full complexity of contacting and non-contacting neighbors (unlike the granocentric model [25]). However, the sharp distinction between monodisperse and polydisperse systems is captured within the present theory and identifies its cause as either positional- or size-disorder.

The same procedure can be used to describe both kinds of disorder in 2D tilings, replacing solid angles by angles and polyhedral cells by polygons. The area-neighbor relationship for polydisperse tilings is

$$\tilde{A}_P = \frac{n}{\sqrt{3}} \csc\left(\frac{2\pi}{n}\right)\left[\sin\left(\frac{\pi}{n}\right) - 1\right]^2 \tag{6}$$

and for monodisperse tilings is

$$\tilde{A}_M = \frac{n}{4\sqrt{3}} \csc\left(\frac{2\pi}{n}\right) \approx 1 + h_M(n-6), \quad (7)$$

where $\tilde{A}_{M,P} \equiv A/\langle A\rangle$ is the cell area normalized to the average area. Employing a linear expansion around $n = \langle n\rangle$ gives a linear relationship between the area and neighbor number with $h_M \approx 0.267$, which may provide an explanation for the empirical Lewis law. Indeed, in Fig. 2 we show a good agreement between the positional disorder prediction in (7) and the Lewis law, as well as their success in fitting data from biological cells and disordered packings of disks. On the other hand, the 2D polydisperse theory, Eq. (6), aligns well with the theoretical prediction of [22] and foam data from [9]. The empirical discrepancy between the two classes of experimental systems can thus be explained through different dominant sources of disorder in these systems.

Another general feature observed in 2D tilings and packings is the relationship between the widths of the distributions of neighbors and local cell volumes, quantified by their respective coefficients of variation $c(n)$ and $c(\tilde{V})$ [10,17,22]. We find that the effects of positional and size disorder on this relationship can be captured quantitatively from the slope g_M in Eq. (5) and from an analogous linearization of Eq. (4) about $\langle n\rangle$ to obtain the slope g_P. The relationships are

$$c(\tilde{V}_P) = \langle n\rangle g_P c(n), \qquad c(\tilde{V}_M) = \langle n\rangle g_M c(n), \quad (8)$$

where for the typical $\langle n\rangle = 14$, we obtain $\langle n\rangle g_P \approx 2.63$ and $\langle n\rangle g_M \approx 1.14$, as shown in Fig. 3(b). These slopes are insensitive to $\langle n\rangle$, varying by less than 2% in the polydisperse case and less than 8% in the monodisperse case, in the range $12 < \langle n\rangle < 16$. Note that for sphere packings, the values of $c(\tilde{V}_P)$ can always be directly related to the polydispersity p by eliminating n from (1) and (2) in favor of ξ. In this case, a linearization obtains

$$c(\tilde{V}_P) = \left(\frac{1}{2} + \frac{1}{\sqrt{3}}\right)p, \quad (9)$$

establishing a direct connection with the particle size distribution. Note, however, that the p values in the figure legends are directly measured in the experiments. Figure 3(b) shows that all experimental data are consistent with either of the two theoretical lines: packings at or above 11% polydispersity follow the steeper slope of the size disorder theory, while those that are quasi or purely monodisperse are in good agreement with the positional disorder theory. This demonstrates that, in contrast to the 2D case [22], a linearization of (4) is sufficient for an accurate description of the experimental data via the size-topology relation (8). While the simplified polydisperse theory predicts crystallization as polydispersity is removed, the full granocentric model captures the crossover from the polydisperse to the monodisperse line, as shown by the dashed line in Fig. 3(b). Indeed, monodisperse 3D systems do not crystallize without thermalization, but rather retain a disordered configuration known as random close packing [27].

In this Letter, we demonstrate that four classes of space-tiling systems, namely biological tissues, foams, compressed emulsions and granular matter, show topological characteristics that can be categorized by the dominant source of disorder through a mean-field approach to the granocentric model. Moreover, the theoretical approach allows any tiling of cells to be mapped onto a corresponding packing of mechanically stable spheres/disks with a statistically equivalent set of navigation map cells. The model, thus, classifies cucumber tissues, quasimonodisperse disks, and PMMA packings as systems in which positional disorder dominates the tiling and foams and emulsions as size disorder dominated tilings. This classification is consistent with the fact that cell size is highly regulated in biological systems, while foams and emulsions typically result from dynamical processes that induce a broad distribution of sizes through e.g. fragmentation, coalescence or coarsening. The success of a purely geometric model in capturing the topology of diverse systems may shed light on the underlying mechanisms leading to their creation.

We thank Eric Vanden-Eijnden, Eric Weeks, and Andy Kraynik for useful discussions and Karen Daniels for access to the experimental bidisperse disk data. J. B. holds a Career Award at the Scientific Interface from the Burroughs Wellcome Fund and was supported in part by New York University Materials Research Science and Engineering Center Grant No. DMR-0820341 and a Career Grant No. 0955621.

[1] M. Clusel, E. I. Corwin, A. O. N. Siemens, and J. Brujić, Nature (London) **460**, 611 (2009).
[2] I. Jorjadze, L.-L. Pontani, K. A. Newhall, and J. Brujić, Proc. Natl. Acad. Sci. U.S.A. **108**, 4286 (2011).
[3] L. Oger, A. Gervois, J. P. Troadec, and N. Rivier, Philos. Mag. B **74**, 177 (1996).
[4] R. Y. Yang, R. P. Zou, and A. B. Yu, Phys. Rev. E **65**, 041302 (2002).
[5] C. Monnereau, B. Prunet-Foch, and M. Vignes-Adler, Phys. Rev. E **63**, 061402 (2001).
[6] A. M. Kraynik, D. A. Reinelt, and F. van Swol, Phys. Rev. E **67**, 031403 (2003).
[7] A. M. Kraynik, D. A. Reinelt, and F. van Swol, Phys. Rev. Lett. **93**, 208301 (2004).
[8] G. L. Thomas, R. M. C. de Almeida, and F. Graner, Phys. Rev. E **74**, 021407 (2006).
[9] J. A. Glazier, M. P. Anderson, and G. S. Grest, Philos. Mag. B **62**, 615 (1990).
[10] C. Quilliet, S. A. Talebi, D. Rabaud, J. Käfer, S. J. Cox, and F. Graner, Philos. Mag. Lett. **88**, 651 (2008).
[11] F. T. Lewis, Anat. Rec. **38**, 341 (1928).
[12] J. C. M. Mombach, M. A. Z. Vasconcellos, and R. M. C. de Almeida, J. Phys. D **23**, 600 (1990).

[13] M. C. Gibson, A. B. Patel, R. Nagpal, and N. Perrimon, Nature (London) **442**, 1038 (2006).
[14] M. A. Fortes, J. Phys. A **28**, 1055 (1995).
[15] S. N. Chiu, Mater. Charact. **34**, 149 (1995).
[16] N. Rivier, G. Schliecker, and B. Dubertret, Acta Biotheoretica **43**, 403 (1995).
[17] M. Durand, J. Käfer, C. Quilliet, S. Cox, S. A. Talebi, and F. Graner, Phys. Rev. Lett. **107**, 168304 (2011).
[18] N. Rivier and A. Lissowski, J. Phys. A **15**, L143 (1982).
[19] C. W. J. Beenakker, Phys. Rev. Lett. **57**, 2454 (1986).
[20] J. R. Iglesias and R. M. C. de Almeida, Phys. Rev. A **43**, 2763 (1991).
[21] M. A. Fortes and P. I. C. Teixeira, J. Phys. A **36**, 5161 (2003).
[22] M. P. Miklius and S. Hilgenfeldt, Phys. Rev. Lett. **108**, 015502 (2012).
[23] N. N. Medvedev, Dokl. Akad. Nauk SSSR **337**, 767 (1994).
[24] S. V. Anishchik and N. N. Medvedev, Phys. Rev. Lett. **75**, 4314 (1995).
[25] K. A. Newhall, I. Jorjadze, E. Vanden-Eijnden, and J. Brujić, Soft Matter **7**, 11518 (2011).
[26] J. Brujić, S. F. Edwards, D. G. Grinev, I. Hopkinson, D. Brujić, and H. Makse, Faraday Discuss. **123**, 207 (2003).
[27] J. L. Finney, Proc. R. Soc. A **319**, 479 (1970).
[28] E. I. Corwin, M. Clusel, A. O. N. Siemens, and J. Brujić, Soft Matter **6**, 2949 (2010).
[29] D. Weaire and J. A. Glazier, Philos. Mag. Lett. **68**, 363 (1993).
[30] E. T. Owens and K. E. Daniels, Europhys. Lett. **94**, 54005 (2011).